Precipitable Water Vapor Variation in the Clear-cloud Transition Zone from the ARM Shortwave Spectrometer

Guoyong Wen and Alexander Marshak

***Abstract*—A new technique to retrieve precipitable water vapor (PWV) amount in the clear-cloud transition zone using ground-based zenith spectral radiance is developed. The method uses zenith radiances at the water vapor band at 720 nm and adjacent non-absorbing band at 750 nm. Radiative transfer calculations show that the relative difference in zenith radiance between the two bands depends on PWV and the variations in cloud optical depth introduce a small change in the relative difference which is independent of PWV amount. This allows us to retrieve PWV variations in the cloud-clear transition zone for clouds over dark ocean surface. We applied this method to a Cu cloud case with zenith radiance observations by the Shortwave Array Spectroradiometer-Zenith (SASZe) during the Marine ARM GPCI Investigation of Clouds (MAGIC) field campaign. We found that there is about 10% change in PWV amount from known-cloudy region to known-clear sky in cloud edges.**

***Index Terms*— Atmosphere, Sensing platforms**

I. Introduction

The transition zone between cloudy and cloud free areas is a special region in the atmosphere. The transition zone is a "gray" area with the particle size and associated optical properties are neither cloud-like nor clear-like. The size of the transition zone ranges from a few hundred meters up to several kilometers (see [1], [2], [3], [4]). In the transition zones, cloud droplets evaporate and shrink, aerosol particles are humidified and swollen, water vapor dilutes as relative humidity decreases from 100% in clouds to environment values away from clouds (see [2], [5], [6], [7]). It was shown [8] that about 50% of clear areas are within 5 km from conventionally identified low-level water clouds. Thus, the transition zone has strong impact on climate forcing (see [2], [9]. It is necessary to better understand the variations of cloud and aerosol properties in the transition zone for improving the estimates of aerosol radiative forcing and reduce the uncertainties in cloud models of entrainment and mixing processes.

Satellite data (e.g., [2], [10], [11]), ground-based observations (e.g., [12], [13]), and aircraft measurements (e.g., [14], [15]) have been used to understand aerosol and cloud properties in a transition zone. Recently, the ground-based shortwave spectrometer observations of the Atmospheric Radiation Measurement (ARM) program have been used to study variations of optical depth and particle size at the cloud edges [16], [17].

The Shortwave Array Spectroradiometer-Zenith (SASZe) is one of the standard instruments of the AMR program [18], [19]. It measures the hyperspectral zenith radiance of scattered radiation within a narrow viewing angle with high sampling frequency, allowing to capture fast processes of cloud-aerosol interactions during mixing and entrainment processes. The shortwave spectrometer observations of ARM have been used to study the radiative properties of the transition zones (e.g., [16], [17], [20], [21], [22]).

The SASZe observations at ARM's SGP site and during the MAGIC campaign over the Pacific Ocean were analyzed to study the variations of optical depth and particle size [17]. However, variability of water vapor at the cloud edges remains a challenging task. We have developed a new technique to retrieve precipitable water vapor amount at cloud edges. In this paper, the method for retrieval of water vapor is presented in section 2. Section 3 demonstrates the application of the technique to SASZe observed zenith spectral radiance. The summary is provided in section 4.

II. Retrieval method

Two solar spectral bands carrying different optical information are useful in atmospheric remote sensing. A pair of non-absorbing and absorbing bands were used to retrieve cloud optical depth and droplet effective radius [23]. This method has been used routinely for cloud retrievals for MODIS, VIIRS, and other spaceborne radiometers. The ground-based zenith radiance observations at a visible and a near-infrared (NIR) bands were used to retrieve optical depth of 3D clouds over vegetation surface [24]. Water vapor and atmospheric window channels were used to retrieve column water vapor amount from airborne and satellite instruments [25], [26].

Same concept can be applied to water vapor retrieval from ground-based solar radiance observations. To derive column PWV amount, we need to find an appropriate water vapor absorbing band together with an adjacent non-absorbing reference band in solar spectrum. There are several water vapor absorption bands in the SASZe wavelength region, including 1.87, 1.38, 1.1, 0.94, 0.82, and 0.72 μm as shown in Fig.1 for the transmittance for clear atmosphere. For retrieving PWV we have chosen the 0.72 μm band. This is because 1.87 and 1.38 μm bands are so strong that little amount of solar radiation can reach the surface and are not useful for retrieving precipitable water vapor amount from ground-based radiometer; in addition, the TOA solar irradiance at the 1.1 and 0.94 μm bands are much weaker than that at 0.72 μm. SASZe observes scattered radiance in zenith direction. From cloudy to cloudless sky, optical depth decreases. In optically thin regime, single scattering dominates and the radiance is proportional to the optical depth (e.g. [27]). Both molecular and aerosol scattering optical depths at longer wavelengths are much smaller than that at 0.72 μm. This will make the scattered zenith radiance at 1.1 and 0.94 μm even smaller compared to 0.72 μm. Though both TOA irradiance and surface radiance at 0.82 μm band is much larger than those at longer wavelengths, the 0.82 μm water vapor band is weaker than 0.72 μm. Thus, the pair of water vapor absorbing band at 0.72 μm together with the adjacent non-absorbing band at 0.75 μm can be considered the optimal choice for water vapor retrieval from zenith looking spectrometer observations.

Manuscript submitted 31 December 2020. (*Corresponding author: Guoyong Wen*.) This research was supported by the Office of Science (BER), U.S. Department of Energy (DOE), under grant DE-SC0018045.

G. Wen is with Morgan State University, Baltimore, MD 21251 USA, and also with the NASA Goddard Space Flight Center, Greenbelt, MD 20771 USA (e-mail: guoyong.wen@nasa.gov).

A. Marshak is with the NASA Goddard Space Flight Center, Greenbelt, MD 20771 USA (e-mail: alexander.marshak@nasa.gov).

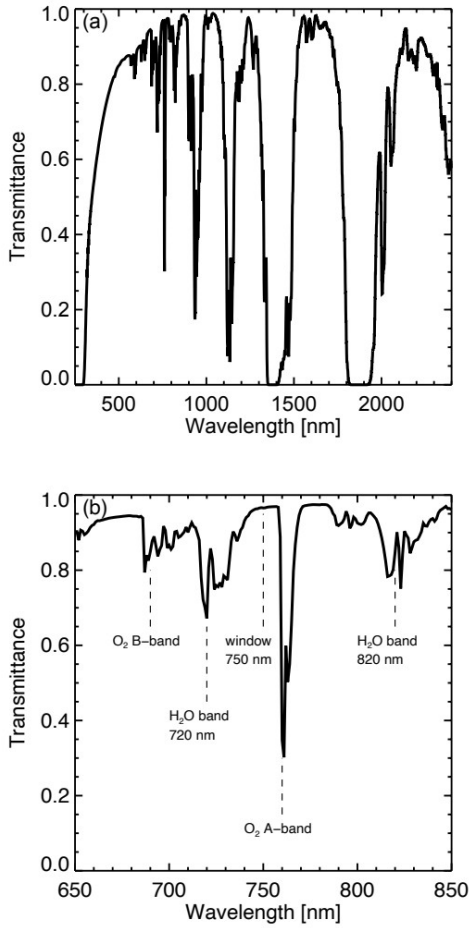

Fig. 1. The atmosphere transmittance as a function of wavelength (300-2400 nm) for a mid-summer latitude atmosphere calculated using SBDART radiative transfer code with MODTRAN-3 solar spectrum, (a) for wavelength region of 300-2400 nm, (b) for wavelength region of 650-850 nm with absorption bands indicated. The solar zenith angle is 20°.

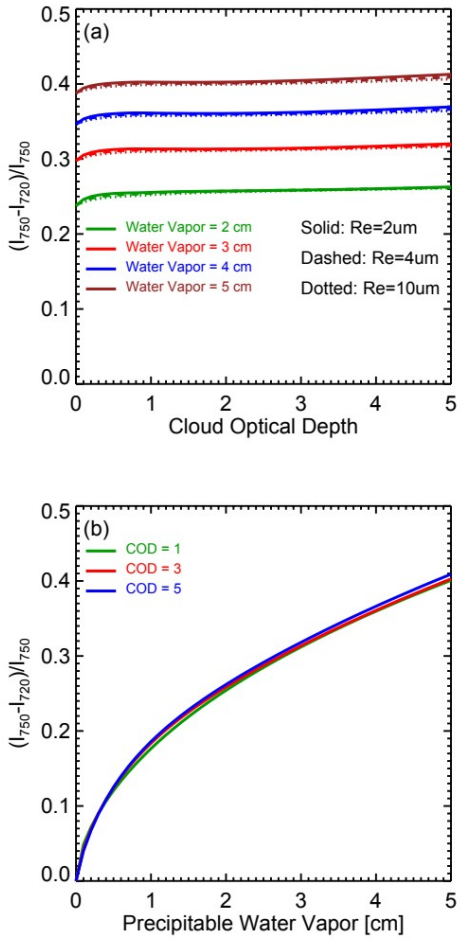

Fig. 2. The results of the radiative transfer calculations using the Santa Barbara DISORT Atmospheric Radiative Transfer (SBDART) code for (a) relative difference in zenith radiances as a function of cloud optical depth for different precipitable water vapor and cloud effective radius; (b) relative difference in zenith radiances as a function of precipitable water vapor amount for different cloud optical depth with effective radius of 4 μm for solar zenith angle of 20° and aerosol optical depth of 0.2.

Since the two bands are so close, the atmospheric scattering properties are similar. The radiance difference between the two bands depends primarily on water vapor amount in the atmosphere. The Santa Barbara DISORT Atmospheric Radiative Transfer (SBDART) radiative transfer code [28] is used to perform a series calculation to demonstrate this fact. Here we focus on boundary layer clouds over dark ocean surface with albedo about 0.03 at 750 nm. Fig. 2a shows radiative transfer calculations for relative difference of zenith radiance between the two bands as a function of cloud optical depth with different effective radii for boundary layer clouds, where the radiance is normalized by the top-of-atmosphere (TOA) incident spectral solar irradiance. Indeed, the relative radiance difference depends mainly on column PWV amount and weakly on cloud optical depth, and is almost independent of effective radius. For given PWV amount, there is slightly increase of about 0.02 in the radiance difference as cloud optical depth increases from 0 to 5. This cloud-induced radiance amount is almost independent of PWV amount. Since cloud edges are not optically thick, this cloud-induced radiance amount may be considered as the upper bound of radiance difference due to changes in cloud optical depth when we focus on PWV in cloud edges.

For a given cloud optical depth, the radiance difference monotonically increases with PWV (Fig. 2b). This allows us to derive the change of PWV from the change in the relative radiance difference.

Here we have shown that the relative radiance difference between 720 and 750 nm bands depends mainly on PWV amount and the radiance difference is monotonically related PWV. The next section describes the application of this technique to SASZe observations.

III. Application to SASZe Observations during MAGIC Field Campaign

SASZe is one of the standard instruments that measure hyperspectral zenith radiance in the AMR program [18], [19]. The light collector incorporates a collimator yielding a 1.0° Full Width at Half Maximum (FWHM) field of view (FOV). The instrument consists of two Avantes fiber-coupled grating spectroradiometers. One radiometer covers the wavelength range about 300-1100 nm with the pixel spacing of less than 0.6 nm and a spectral resolution of about 2.4 nm FWHM, while the other covers the spectral range about 950-2100 nm with a pixel spacing of less than 4 nm and a spectral

resolution of about 6-nm FWHM. The instrument sampling frequency is 1 Hz, approximately corresponding to a spatial resolution of several meters depending on the horizontal wind speed and the altitude of cloud. Figure 3 shows an example of zenith radiance spectrum observed by SASZe. The high sampling frequency spectral radiance observations from SASZe were used to study the variations of cloud optical depth and droplet size at cloud edges [16], [17]. Here we apply the new technique to study column PWV at the cloud edges.

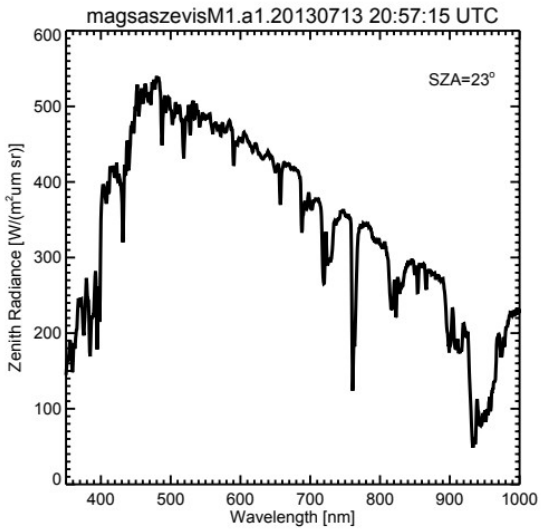

Fig. 3. An example of spectral zenith radiance observed by SASZe during MAGIC campaign on July 13, 2013. Solar zenith angle is 23˚.

We used SASZe zenith radiance measurements during the Marine ARM GPCI Investigation of Clouds (MAGIC) field campaign [29] to test the technique. The MAGIC is the Global Energy and Water Cycle Experiment (GEWEX) Cloud Systems Study Investigation of Clouds field campaign. The ARM Program Mobile Facility 2 (AMF2) has been deployed on the commercial cargo container ship from October 2012 to September 2013 with 20 round trips. The MAGIC transect is the line from Los Angeles, California (33.7°N, 118.3°W) to Honolulu, Hawaii (21.3° N, 157.9° W). MAGIC provided unprecedented, intraseasonal, high resolution ship-based observations in order to improve understanding of the Sc-to-Cu (stratocumulus-to-cumulus) transition along this transect. The AMF2 contained a state-of-the-art instrumentation suite and was designed to operate in a wide range of climate conditions and locations, including shipboard deployments.

A cumulus cloud case during MAGIC campaign, case M10 in [17], is selected to demonstrate the application of the technique for estimating the variability of PWV amount at cloud edges. The cloud base is about 0.8 km with a thickness of 1.2 km (cloud top of 2 km). The cloud fraction derived from total sky imager [30] is 38%. The width of cloud edges is about 140 m. More detailed information about this case is described in [17].

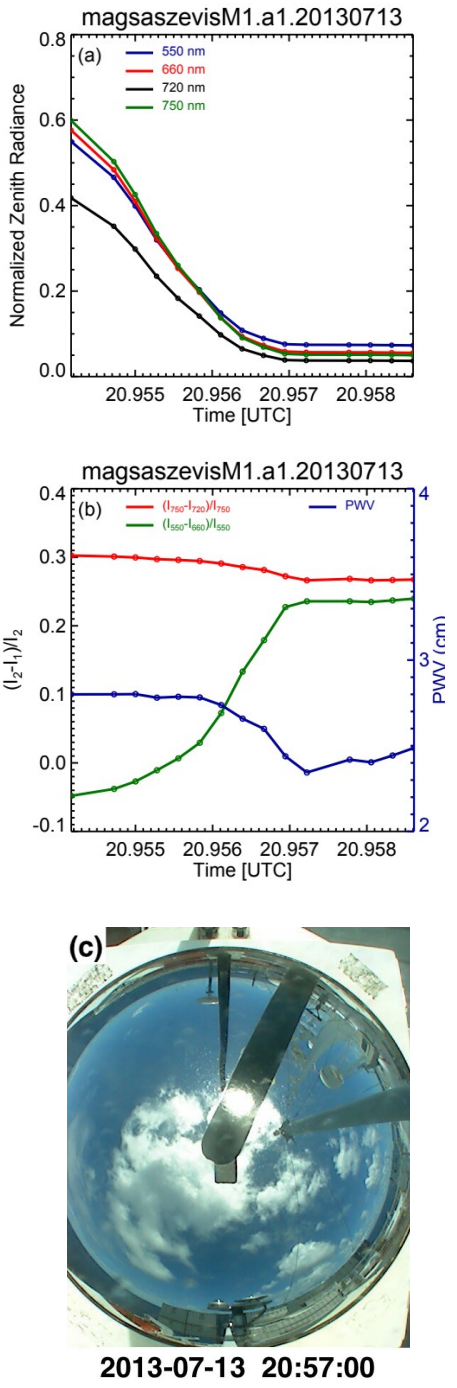

Fig. 4. (a) An example of SASZe observed normalized zenith radiances for four wavelength bands at about 20:57 UTC on 13 July 2013 at 22.2˚ N, 155.4˚ W; (b) variations of the relative radiance difference for two pairs of wavelengths (550 – 660 nm and 720 – 750 nm) and retrieved PWV; (c) corresponding TSI image.

The variations of zenith spectral radiances (with 5-second moving average) normalized by TOA spectral irradiance multiplied by cosine of solar zenith angle, the relative radiance difference, and corresponding image from TSI are presented in Fig. 4. Following the procedure in [17], the *known-cloudy* and *known-clear* regions are determined at the beginning (~20.9552 UTC) and the end (~ 20.9586 UTC) of the time series (Fig. 4a, b), respectively. It is evident that the known-cloudy regions are characterized by large zenith radiances

about 0.6 for three water vapor non-absorbing bands because of more scatterers and smaller radiance about 0.4 for the water vapor absorbing band, while the known-clear sky is characterized by small zenith radiance for all bands. The radiances for all bands decrease toward cloud edges as a result of a decrease in optical depth. It is important to note that the radiance at 720 nm is always smaller than those for non-absorbing bands. Fig. 4b shows the variations of relative radiance difference. In definite cloudy regions, the relative radiance difference for two non-water vapor absorbing bands (550 nm and 660 nm) is close to zero. From known-cloudy to know-clear sky, there is about 30% increase in the relative difference, and the difference become less variable near the known-clear area (Fig. 4b). Based on the spectral invariant technique, the study [17] showed the decrease of droplet size toward cloud edges. In known-cloudy regions, the light scattering is approximately in geometric regime and normalized radiance depends weakly on wavelength. In known-clear sky areas, Rayleigh scattering optical depth depends strongly on wavelength; the wavelength dependence of aerosol scattering is much stronger than cloud scattering depending on particle size of aerosols – the smaller the aerosol particles the stronger the wavelength dependence. Thus, the large increase of the relative radiance difference in the two visible bands indicates the decrease in particle size toward cloud edge and it is consistent with the results in [17].

With smaller wavelength difference, the variation of relative radiance difference between 750 nm and 720 nm is much smaller than its counterpart for 550 and 660 nm bands. Unlike 550 and 660 nm bands, the relative radiance difference between 750 nm and 720 nm varies rather linearly with time (or distance) toward cloud edges. From the known-cloudy region to the known-clear area, the relative radiance difference decreases from ~0.3 to ~0.26, i.e., a decrease of 0.04. We also need to consider the decrease of the relative difference that is due to other factors not to water vapor. Radiative transfer model calculations show that there is a decrease of about 0.02 in the relative difference due to change of cloud optical depth from 5 to 0. This decrease is independent of PWV amount as shown in Fig. 2a. Since cloud edges are not optically thick, this decrease may serve as the upper bound of the decrease due to cloud optical depth changes at cloud edges, not due to changes water vapor amount. The cloud induced decrease is subtracted from observed relative difference to estimate the radiance difference attributed mainly to the change in water vapor amount from known-cloudy to known-clear sky. We further use the pre-calculated relationship between the radiance difference and PWV amount (Fig. 2b) and cloud effect removed relative radiance difference to estimate the change in PWV (Fig. 4b). From known-cloudy to known-clear sky there is a decrease of ~0.3 cm in PWV, about 10% decrease. It is important to note that the PWV amount of 2.5 – 2.8 cm retrieved from this method is consistent with the microwave radiometer retrieved PWV amount of 2.6 – 2.8 cm in the same time period.

IV. Concluding Remarks

The transition zone between cloudy and cloudless skies is characterized by the decreasing of optical depth, shrinking of cloud droplets, swelling of aerosol particles, and reducing relative humidity with the distance from the cloudy region. This is the result of turbulence mixing of clouds with dry air. Earlier studies have focused on variations of optical depth and particle size in the cloud edges using shortwave spectrometer observations. Hyperspectral SASZe instrument measures zenith radiance with 1 Hz sampling rate, allowing us the retrieve column precipitable water vapor amount. We have developed a new technique to retrieve column water vapor amount at the edges of boundary layer clouds over dark ocean from ground-based zenith radiance observations at two wavelengths, i.e., a water vapor absorbing band 720 nm and a non-absorbing band at 750 nm. Because the two bands are so close, the relative zenith radiance difference depends mainly on column water vapor amount. And the relative radiance difference has a simple monotonic relation with column water vapor amount. Thus, the observed changes in the relative radiance difference can be used to estimate the column water vapor amount.

The proposed water vapor retrieval algorithm for SASze observations is summarized as following: (1) find low level one-layer water clouds and determine known-clear and known-cloud regions using TSI image, ceilometer observations, and SASZe spectra as described in [17]; (2) normalize the SASZe observed zenith spectral radiances at the two bands by TOA solar irradiance; (3) estimate the change of the relative radiance difference from known-cloud region to known-clear region; (4) subtract 0.02 due to changes of cloud optical depth at cloud edges from the observed change to get the relative radiance difference due to water vapor absorption; (5) estimate the change of column water vapor at the cloud edges by using the changes in the relative radiance difference from step (4) and pre-calculated relationship between column water vapor and the relative radiance difference (e.g. Fig. 2b).

It is important to note that this method applies to clouds over dark ocean surface. We have applied this method to a Cu cloud case during MAGIC campaign. We found that there is a decrease of about 0.3 cm in column water vapor amount from known-cloud to known-clear regions; it is about 10% decrease in column water vapor amount. We will apply this method to more cases to better understand the statistics of water vapor variation in Cu cloud edges and plan to investigate the impacts of different aerosol loading, vertical profiles of water vapor, vertical locations of cloud and 3D radiative effects on the accuracy of retrieval.

Acknowledgment

We thank two anonymous reviewers whose comments helped improve and clarify this paper. We thank T. Várnai for insightful discussions on the transition zone. Data were obtained from the Atmospheric Radiation Measurement (ARM) user facility (https://www.arm.gov/data), a U.S. Department of Energy (DOE) Office of Science user facility managed by the Biological and Environmental Research Program.

References

[1] T. Várnai and A. Marshak, “Global CALIPSO observations of aerosol changes near clouds,” *IEEE Geoscience and Remote Sensing Letters*, vol. 8, no. 1, pp. 19–23, Jan. 2011. https://doi.org/10.1109/LGRS.2010.2049982

[2] I. Koren, L. A. Remer, Y. J. Kaufman, Y. Rudich, and J. V. Martins, “On the twilight zone between clouds and aerosols,” *Geophysical Research Letters*, vol. 34, no. L08805, Apr. 2007. https://doi.org/10.1029/2007GL029253

[3] K. D. Perry and P. V. Hobbs, “Influences of isolated cumulus clouds on the humidity of their surroundings,” *Journal of the Atmospheric Sciences*, vol. 53, no. 1, pp. 159–174, Jan. 1996. https://doi.org/10.1175/1520-0469(1996)053<0159:IOICCO>2.0.CO;2

[4] M. Lu, J. Wang, R. C. Flagan, J. H. Seinfeld, A. Freedman, R. A. McClatchey, and H. H. Jonsson, “Analysis of humidity Halos around trade wind cumulus clouds,” *Journal of the Atmospheric Sciences*, vol. 60, no. 8, pp. 1041–1059, Apr. 2003. https://doi.org/10.1175/1520-

0469(2003)60<1041:AOHHAT>2.0.CO;2

[5] I. Koren, G. Feingold, H. Jiang, H., and O. Altaratz, "Aerosol effects on the inter-cloud of a small cumulus cloud field," *Geophysical Research Letters*, vol. 36, no. L14805, Jul. 2009. https://doi.org/10.1029/2009GL037424

[6] D. Chand, R. Wood, S. J. Ghan, M. Wang, M. Ovchinnikov, P. J. Rasch, et al., "Aerosol optical depth increase in partly cloudy conditions," *Journal of Geophysical Research*, vol. 117, no. D17207, Sept. 2012. https://doi.org/10.1029/2012JD017894

[7] J. Zhang, J. S. Reid, and B. N. Holben, "An analysis of potential cloud artifacts in MODIS over ocean aerosol optical thickness products," *Geophysical Research Letters*, vol. 32, no. L15803, Aug. 2005. https://doi.org/10.1029/2005GL023254

[8] T. Várnai and A. Marshak, "Satellite Observations of Cloud-Related Variations in Aerosol Properties," *Atmosphere*, vol. 9, no. 430, Nov. 2018. [10.3390/atmos9110430]

[9] R. J. Charlson, A. S. Ackerman, F. A.-M. Bender, T. L. Anderson, and Z. Liu, "On the climate forcing consequences of the albedo continuum between cloudy and clear air," *Tellus*, vol. 59, no. 4, pp. 715–727, Aug. 2007. https://doi.org/10.1111/j.1600-0889.2007.00297.x

[10] T. Várnai and A. Marshak, "MODIS observations of enhanced clear sky reflectance near clouds," *Geophysical Research Letters*, vol. 36, no. LO6807, Mar. 2009. https://doi.org/10.1029/2008GL037089

[11] E. Eytan, I. Koren, O. Altaratz, *et al.*, "Longwave radiative effect of the cloud twilight zone," *Nat. Geosci.*, vol. 13, pp. 669–673, Aug. 2020. https://doi.org/10.1038/s41561-020-0636-8

[12] M. Jeong and Z. Li, "Separating real and apparent effects of cloud, humidity, and dynamics on aerosol optical thickness near cloud edges," *Journal of Geophysical Research*, vol. 115, no. D00K32, Dec. 2010. https://doi.org/10.1029/2009JD013547

[13] T. Eck, B. N. Holben, J. S. Reid, *et al.*, "Observations of rapid aerosol optical depth enhancements in the vicinity of polluted cumulus clouds," *Atmos. Chem. Phys.*, vol. 14, pp. 11633-11656, Nov. 2014. [10.5194/acp-14-11633-2014]

[14] J. Redemann, Q. Zhang, P. B. Russell, J. M. Livingston, and L. A. Remer, "Case studies of aerosol remote sensing in the vicinity of clouds," *Journal of Geophysical Research*, vol.114, no. D06209, Mar. 2009. https://doi.org/10.1029/2008JD010774

[15] W. Su, G. L. Schuster, N. G. Loeb, R. R. Rogers, R. A. Ferrare, C. A. Hostetler, et al., "Aerosol and cloud interaction observed from high spectral resolution lidar data," *Journal of Geophysical Research*, vol. 113, no. D24202, Dec. 2008. https://doi.org/10.1029/2008JD010588

[16] W. Yang, A. Marshak, P. J. McBride, J. C. Chiu, Y. Knyazikhin, K. S. Schmidt, et al., "Observation of the spectrally invariant properties of clouds in cloudy-to-clear transition zones during the MAGIC field campaign," *Atmospheric Research*, vol. 182, pp. 294–301, Aug. 2016. https://doi.org/10.1016/j.atmosres.2016.08.004

[17] W. Yang, A. Marshak, and G. Wen, "Cloud edge properties measured by the ARM shortwave spectrometer over ocean and land," *Journal of Geophysical Research: Atmospheres*, vol. 124, pp. 8707–8721, Aug. 2019. https://doi.org/10.1029/2019JD030622

[18] C. J. Flynn, "Shortwave Array Spectroradiometer–Zenith Instrument Handbook," Ed. by Robert Stafford, DOE ARM Climate Research Facility. DOE/SC-ARM-TR-178, 2016. [Online]. Available: https://www.arm.gov/publications/tech_reports/handbooks/sasze_handbook.pdf

[19] L. D. Riihimaki, *et al.*, "The Shortwave Spectral Radiometer for Atmospheric Science: New Capabilities, Applications, and Experience from the ARM User Facility", *Bulletin Amer. Meteor. Soc. (BAMS),* published-online, Oct. 2020. DOI: https://doi.org/10.1175/BAMS-D-19-0227.1

[20] A. Marshak, Y. Knyazikhin, J. C. Chiu, and W. J. Wiscombe, "Spectral invariant behavior of zenith radiance around cloud edges observed by ARM SWS," *Geophysical Research Letters*, vol. 36, no. L16802, Aug. 2009. https://doi.org/10.1029/2009GL039366

[21] J. C. Chiu, A. Marshak, Y. Knyazikhin, P. Pilewskie, P., and W. J. Wiscombe, "Physical interpretation of the spectral radiative signature in the transition zone between cloud-free and cloudy regions," *Atmospheric Chemistry and Physics*, vol. 9, pp. 1419–1430, Feb. 2009. https://doi.org/10.5194/acp-9-1419-2009

[22] J. C. Chiu, A. Marshak, Y. Knyazikhin, and W. J. Wiscombe, "Spectrally-invariant behavior of zenith radiance around cloud edges simulated by radiative transfer," *Atmospheric Chemistry and Physics*, vol. 10, pp. 11,295–11,303, Nov. 2010. https://doi.org/10.5194/acp-10-11295-2010

[23] T. Nakajima and M. D. King, "Determination of the optical-thickness and effective particle radius of clouds from reflected solarradiation measurements. Part 1: Theory," *J. Atmos. Sci.*, vol. 47, no. 15, pp. 1878–1893, Aug. 1990.

[24] A. Marshak, Y. Knyazikhin, A. Davis, W. J. Wiscombe, and P. Pilewskie, "Cloud-vegetation interaction: Use of normalized difference cloud index for estimation of cloud optical thickness," *Geophys. Res. Lett*., vol. 27, no. 12, pp. 1695-1698, Jun. 2000. [10.1029/1999GL010993]

[25] B. -C. Gao and A. Goestz, "Column atmospheric water vapor and vegetation liquid water retrievals from airborne imaging spectrometer data", vol. 95, no. D4, pp. 3549-3564, Mar. 1990.

[26] B. -C. Gao and Y. J. Kaufman, "Water vapor retrievals using Moderate Resolution Imaging Spectroradiometer (MODIS) near-infrared channels," *J. Geophys. Res.*, vol. 108, no. D13, 4389, 2003. doi:10.1029/2002JD003023.

[27] Y. J. Kaufman, D. Tanré, L. A. Remer, E. Vermote, A. Chu, and B. N. Holben, "Operational remote sensing of tropospheric aerosol over land from EOS Moderate Resolution Imaging Spectroradiometer," *J. Geophys. Res.*, vol. 102, no. D17, 17,051–17,067, 1997.

[28] P. Ricchiazzi, S. Yang, C. Gautier, and D. Sowle, "SBDART: A research and teaching software tool for plane-parallel radiative transfer in the Earth's atmosphere," *Bulletin of the American Meteorological Society*, vol. 79, no. 10, 2101–2114, 1998. https://doi.org/10.1175/1520-0477(1998)079<2101:SARATS>2.0.CO;2

[29] E. R. Lewis, "Marine ARM GPCI Investigation of Clouds (MAGIC) field campaign report," Ed. by Robert Stafford, DOE ARM Climate Research Facility. DOE/SC-ARM-16-057, 2016. [online] Available: https://www.arm.gov/research/campaigns/amf2012magic

[30] V. R. Morris, "Total sky imager (TSI) handbook," U.S. Department of Energy. DOE/SC-ARM/TR-017, 2005. [online] Available: https://www.arm.gov/publications/tech_reports/handbooks/tsi_handbook.pdf